OPTIMIZED SYNTHESIS OF BINARY TRANSITION METAL CHALCOGENIDE 2D NANOSTRUCTURES FOR ENERGY APPLICATIONS

By

Muhammad Tayyab Shuja

Syed Hasnain Ali Pirzada

Syed Omer Aamir

School of Chemical and Materials Engineering

National University of Sciences and Technology

2022

OPTIMIZED SYNTHESIS OF BINARY TRANSITION METAL CHALCOGENIDE 2D NANOSTRUCTURES FOR ENERGY APPLICATIONS

By

Leader – 262445 Syed Hasnain Ali Pirzada

Member 1 – 261587 Muhammad Tayyab Shuja

Member 2 – 241985 Syed Omer Aamir

A THESIS

Submitted to
National University of Sciences and Technology
In partial fulfillments of the requirements
for the degree of

METALLURGICAL AND MATERIAL ENGINEERING

School of Chemical and Materials Engineering (SCME)

National University of Sciences and Technology (NUST)

June, 2022

CERTIFICATE

This is to certify that work in this thesis has been completed by Mr. Muhammad Tayyab Shuja, Mr. Syed Hasnain Ali Pirzada and Mr. Syed Omer Aamir under the supervision of Dr. Zeeshan Ali and Dr. Mohsin Saleem at the School of Chemical and Materials Engineering (SCME), National University of Science and Technology, H-12, Islamabad, Pakistan.

Advisor:
Dr. ----------
Department of Materials Engineering
School of Chemical and Materials Engineering
National University of Sciences and Technology

Co-Advisor (if any)
Dr. ----------
Department of Materials Engineering
School of Chemical and Materials Engineering
National University of Sciences and Technology

Submitted Through:

HOD----------

Department of Materials Engineering
School of Chemical and Materials Engineering
National University of Sciences and Technology

Principal/Dean ----------
School of Chemical and Materials Engineering
National University of Sciences and Technology

DEDICATION

We dedicate this dissertation to our loving family and friends without whose support this project would not be possible. A special thanks to our dear parents whose efforts and very existence has allowed us to reach this point.

ACKNOWLEDGEMENTS

This thesis has been led to completion with the unflinching support of our dear educator and supervisor, Dr. Zeeshan Ali whose words of wisdom and guidance allowed us to undertake every step of the project. Without his diligence, we would not have been able to employ our capabilities to the fullest.

Special thanks to Mr. Ali Arshad for his continued support in dealing with any issues that may arise and for sparing his time through the course of this project.

Finally, we would like to thank our tutors and colleagues for their thoughtful discussions that helped us to seek better solutions.

ABSTRACT

This study primarily focuses on the exploration of efficient energy storage alternatives to Lithium-ion batteries in the form of Sodium ion batteries. Using a surfactant assisted solution method aimed at synthesizing 2D nanostructured binary metal chalcogenides and assembly of Sodium ion batteries with Binary Transition Metal Selenides as anode materials due to their high theoretical capacities, rich redox reactions, and good reversibility.

Li-ion batteries are the standard for and employed in conventional usage throughout our current modern society majorly due to their high energy densities and ability to be used at a large scale.

To the best of our knowledge, there has been no significant publication on Fe-Cu based TMSs. We hope to optimize the synthesis of Fe-Cu based selenides in such a way as to get a nanostructure that results in the best electrochemical performance as an anode material. For this purpose, we are employing a bottom-up approach of a surfactant-assisted solution method followed by their Selenization to synthesize selenides with varying combinations of Fe and Cu in terms of their molar ratios.

TABLE OF CONTENTS

LIST OF TABLES

LIST OF FIGURES

CHAPTER 1

INTRODUCTION

1.1 General

1.1.1 Global Energy Crisis

Energy crises are defined as a period of energy scarcity caused by ever-increasing demand on the worldwide market with advancements in technology. One of the key causes of these problems is the increasing population's desire for additional energy resources. When compared to demand, energy supply is always less. In most nations, renewable energy is currently underutilized. The majority of the energy is derived from non-renewable sources such as coal. As a result, it remains the best option for generating energy. The energy dilemma will not be solved unless we give renewable energy considerable attention. Renewable energy sources can help us lessen our reliance on fossil fuels while simultaneously lowering our carbon footprint.

1.1.2 Energy Storage

To eliminate imbalances between energy demand and production, there needs to be a means for storing energy. Energy storage is the collection of energy produced at one moment for use at a later time. A battery is a device that stores energy. Radiation, chemical, gravitational potential, electrical potential, electricity, increased temperature, latent heat, and kinetic energy are all examples of energy. Energy storage entails transferring energy from difficult-to-store forms to easier and most cost-effective forms. A very common means of energy storage is the rechargeable battery, which stores chemical energy that can be converted to electricity. Another example is the hydroelectric dam, which stores energy as gravitational potential energy in a reservoir and ice storage tanks, which store ice frozen by cheaper energy at night to meet peak daytime cooling demand. Coal and gasoline are fossil fuels that contain ancient energy received from sunlight by creatures that perished, were buried, and were subsequently changed into these fuels through time. There is a need to optimize energy storage for higher capacities and higher efficiencies at lower costs.

1.2 Lithium-ion batteries as a source of Energy storage

Li-ion batteries, have one of the highest energy densities out of any battery today, this means they can deliver large amounts of current for applications that require high power. Additionally, Li-ion batteries do not require scheduled cycling to maintain their battery life. Li-ion batteries have no memory effect, which is a harmful phenomenon in which a battery can 'remember' a decreased capacity after repeated partial discharge/charge cycles. Much of the promise of Li-ion technology in terms of renewable energy derives from its prospective uses in battery-powered cars. The most popular electric cars in the world today, employ Li-ion batteries as their primary fuel source. The energy capacity of batteries determines the performance of electric hybrid vehicles. In this context, lithiumion (Li-ion) batteries are getting prominence due to their higher energy storage capacity than traditional lead-acid batteries.

1.2.1 Limitations of Lithium

Li-ion batteries, despite their technological potential, have a number of flaws, significantly in relation to safety. Li-ion batteries have a susceptibility for overheating and are vulnerable to damage at high voltages. This can result in thermal runaway and combustion in some situations. Safety systems for lithiumion batteries are required to regulate voltage and internal pressures, which can increase weight and performance in some circumstances. Li-ion batteries are also susceptible to ageing, which means they lose capacity and commonly fail over time. Another huge factor limiting their widespread utilization is the high cost of Lithium.

1.2.2 Extraction of Lithium

Lithium salts can be found in brine, mineral ore, and clay deposits underground, as well as in seawater and geothermal well brines/water. To reach subsurface reserves of lithium-rich minerals or brines, most lithium extraction procedures require some type of mining. Therefore, vast majority of it is mined from a mineral-rich brine ten metres beneath salt lakes of high-altitude salt flats. Drilling deep through the crust is followed by pumping the brine to the surface and storing

it in evaporation pools for months at a time. This results in a salty mud containing manganese, potassium, borax, and lithium salts, which is then transferred to another open-air evaporation pool. The combination is sufficiently distilled after 12-18 months to separate lithium carbonate, the primary raw material utilised in lithium-ion batteries.

Another method of extracting Lithium is the hard rock extraction method. Mineral ore deposits contain more lithium than salar brines, but they are more expensive to get since they must be mined from hard rock formations. Because of the additional energy, chemicals, and materials required to extract lithium from mineral ore, the method can cost twice as much as brine recovery. This high cost coupled with the exponentially increasing demand, leads to the following problem.

1.2.3 Demand and Supply of Lithium

With Lithium being established as one of the top preferences for battery applications in various industries ranging from the automotive industry to the mobile phone industry. In the coming years, we are prone to face Lithium supply shortages due to its high cost of extraction in nature and increasing utilization as illustrated in [1, Fig. 1]. Lithium must be produced in its purest form, which raises the cost of production. These metals are refined and converted into high-purity chemical compounds. It is important to note however, that the potential risk of supply deficit of Lithium-ion batteries does not stem from the scarcity of Lithium as an element, but more-so, from the time consuming and expensive methods of extraction of this metal, being unable to keep up with the skyrocketing demand [4].

Fig. 1. Lithium Demand and Supply Forecast 2015-40

1.3 Sodium Ion batteries as a source of energy storage

Sodium being one of the most abundantly available metals in the world offers huge untapped potential for energy applications. SIBs (Na-ion batteries) are an intriguing new electrochemical energy storage system that has recently received a lot of attention. Because of their high energy density, longer cycle life, and greater cycling stability, they are one of the strong alternative options to consider when replacing Li-ion batteries [2]. Sodium-ion batteries are also viable means of energy storage, mainly for large-scale electric storage applications, due to the following reasons: (1) low cost of sodium, compared to that of lithium; (2) similar chemistry and intercalation kinetics to that of Lithium; (3) the irreversible capacity of carbon anodes in Sodium-ion batteries is less than in lithium-ion batteries [3].

1.3.1 Limitations of Sodium

A major problem remains to be solved before they can be effectively commercialized and scaled: the high-volume changes of electrodes during intercalation and the cycling efficiency of Sodium-ion batteries is not well-known,

mostly due to the fact that the rate capability obtained from hard carbon anodes is poor. This is due to the fact that Na^+ ions are larger than Li^+ ions, and do not fit readily in a Graphite host [3].

1.3.2 Extraction of Sodium

The extraction of Sodium is mainly carried out by employing two processes. The Downs Process, which involves the electrolysis of Sodium Chloride. And the Castner process, which involves the electrolysis of caustic soda.

1.3.2.1 Down's Process

Using a Graphite anode and a ring-shaped Iron cathode, molten Sodium Chloride (common salt) is electrolyzed. A wire gauge divider separates the two electrodes to prevent the Sodium and Chlorine from combining. Chlorine is liberated at the Carbon anode by passing electric current and escapes via the dome-shaped steel hood outlet. The cathode emits Sodium, which is trapped in the wire gauze shell. The sodium that is created is molten. It rises to the surface because it is lighter than the electrolyte. The molten Sodium is driven into the receiver as the level rises. The process is ongoing, with additional salt added to keep the molten electrolyte level high enough for sodium to ascend into the iron pipe. As a result of this process, the Sodium obtained is of very high purity and the process itself is quite economical due to the low cost of Sodium Chloride.

1.3.2.2 Castner's Process

An Iron cathode and Nickel anode are used to electrolyze molten Sodium Hydroxide (caustic soda, NaOH). The electrodes are kept from touching each other by a Nickel wire gauze cylinder. Sodium is liberated at the cathode and Oxygen is liberated at the anode when an electric current is passed through the melt. The Sodium metal that has been freed floats on the surface due to being less dense. It gathers inside the receiving vessel, preventing the oxidation of Sodium. The excess gas escapes through the outlet. With the use of perforated spoons, sodium is taken from time to time and stored in kerosene oil.

1.3.3 Demand and Supply of Sodium

Unlike its counterpart in Lithium, the Sodium extraction process is less time consuming and much more economical. This coupled with its great abundance, could potentially prove to be a great alternative for energy storage. If the untapped potential of Sodium can be realized. As a direct consequence of Sodium ion batteries being viable options for energy storage, it is not unreasonable to predict that the strain on Lithium reserves will be lessened and the disparity between supply and demand of Lithium will also be reduced as a consequence.

1.4 Problem Statement

There's a need to research and synthesize a material to effectively store Sodium ions for battery applications, with good cyclic stability and conductivity. Without high volume changes of electrodes during the intercalation storage mechanism.
To rectify this, a conversion based energy storage mechanism will be studied.

1.5 Purpose

The purpose of our research is to discover cheap energy storage options in the shape of sodium ion batteries to allow the exploitation of renewable energy resources.

1.6 Objectives

In order to achieve this purpose, we have outlined four primary objectives.

- The first objective is the selection of economical combinations of metals for Binary-Transition Metal Selenides (B-TMSe) synthesis.
- The second objective is the Synthesis of 2D nanostructured B-TMSe on a lab scale
- Our third objective is Characterization of the synthesized material to determine its morphology using X Ray Diffraction, surface area and verify the formation of desired 2D Sheet-like nanostructures.
- Finally, the fourth objective is to perform the Electrochemical testing of the B-TMSe to determine the battery capacity, cyclic stability, efficiency, and rate capability.

1.7 Literature Review

1.7.1 Introduction

With the intent to delve into the domain of energy storage through the eyes of materials sciences and engineering, we took one of the majorly discussed topics in the scientific community as our starting point: Li-ion batteries.

1.7.2 Li Ion Battery

Because of their high energy densities and capacity to be used on a big scale, Liion batteries have become the standard for and are used across our contemporary modern culture. Despite this, we are likely to confront Lithium reserve shortages in the coming years due to expensive and time-consuming extraction and the rising use of electrochemical storage sources as technology and industry improve.

1.7.3 Sodium Ion Battery

Sodium ion batteries, however, prove as good alternatives to LIBs. This is owing to their widespread availability and low cost (almost half the price of LIBs on average). However, before they can be properly sold and scaled, they must solve a major problem: the electrodes' high-volume fluctuations during intercalation[4].

1.7.4 Transition Metal Chalcogenides

We looked into some alternatives that didn't involve intercalation (as in the case of graphite anodes), but instead used alloying or conversion mechanisms in anodes [5]. Transition metal chalcogenides have recently received attention as prospective SIB anode materials. This is owing to their strong theoretical capacities and simplicity of synthesis, not only because they involve conversion [6], [7].

On the other hand, TMCs have their own set of issues, including self-pulverization (due to frequent high-volume fluctuations), low intrinsic conductivities (because of their nature), and unfavorable anode-electrolyte side interactions.

1.7.6 Nanostructures

To rectify such problems, TMCs are being synthesized in the form of 2D and 3D nanostructures. Many examples over the years have proven that the TMC nanostructures perform much better and have improved electrochemical properties compared to their bulk counterparts. These nanostructured samples also produce less stresses during sodiation/desodiation [7]. Ideally, we want to obtain 2D Sheet-like morphology with nanoparticles on top of their surfaces to maximize surface area.

For the development of such 2D-nanostructures (which includes nanosheets as well as nanoparticles on nanosheets formation), many different approaches have been established in the past. Some rely on self-assembling nanoparticles into nanosheets [8], some on the use of co-solvents as the main driving force behind nanosheet formation [9] and some on a form of solvo-thermal method [10]. The main phenomenon is anisotropic growth driven by some dispersions (such as Au nanoparticles) [11] or solvents (such as ionic liquids) [12]. The use of CTAB as a surfactant that acts as a stabilizer and catalyst for Au nanoparticles has been demonstrated by Cheng et al. [13] and Khan et al. [14].

1.7.7 Chalcogenides

Oxygen, Sulphur, Selenium, and Tellurium are all members of the Chalcogenide family of elements. In terms of main features and chemical behaviour, Oxygen is chemically unique from the other chalcogenides. Te is the most expensive and uncommon of the other elements, making commercialization unlikely and even research impractical. As a result, we're looking at sulphides or selenides as potential possibilities for this application. Sulphur is less expensive and easier to come by than Selenium. Binary metal sulphides have garnered considerable attention, but selenides in SIBs have received a lot of attention as well. In terms of electrochemical characteristics, Selenium and Sulphur are nearly identical. Se, on the other hand, has a higher electrical conductivity than Sulphur. Not only that, but Selenium also has a higher molecular weight which leads to easier reversibility in SIBs charge-discharge cycles [15].

1.7.7 Binary Transition Metal Chalcogenides

The question arises as to why binary transition metal chalcogenides should be used as anodes. When compared to mono metal chalcogenides, they have higher intrinsic conductivities and richer redox processes, which led to this decision. Also, the solution method thus employed for 2D B-TMSs nanostructures is facile, can be carried out at room temperature with minimal setup and simpler configuration with potential ease of scalability. Moreover, the precursors employed are easily available and easy to store [16].

1.7.8 Research

Over the years, there has been notable studies on different elements in TMCs as anodes including Mo, Ni, Sn, Co etc. Selenides based on Fe-Co and Fe-Ni have also been studied extensively [15]. To the best of our knowledge, no important publication on Fe-Cu based TMSs has been made.

There have been no specific investigations on the combined electrochemical effects of two of the most important elements on Earth with large abundance in resources and good electrical properties in B-TMSs as anode materials for SIBs. To synthesis selenides with various combinations of Fe and Cu, we are using the bottom-up technique of the surfactant-assisted solution method (in terms of their molar ratios). We seek to improve the synthesis of Fe-Cu based selenides such that SIBs as anode materials have the greatest possible electrochemical performance.

CHAPTER 2

METHODOLOGY

2.1 Overview

Many different methods have existed for the formation of active materials' synthesis in the past. Moreover, for 2D-nanostructures specifically, there have existed many different approaches. The main focus or aim with such approaches has been a cost-effective method that is also scalable and yields quality product. The product is synthesized with the intent to get the maximum performance out of it as the respective cell's active material.

For the purpose of our concerned binary transition metal Selenides, we are employing a simple solution method that involves the preparation of a solution of two different precursors for metals along with surfactant that is then reduced by a standard reducing agent. The resulting solution is then washed and dried and the powders separated.

The vacuum-dried powder particles so obtained are carried out through a Selenization reaction where they react with black Selenium powder in a tube furnace through a heating cycle of 9.5 hours to get our final selenide product as illustrated in [16, Fig. 2].

However, before setting out to carry out the required synthesis, a major prerequisite step was necessary i.e. the selection of appropriate combination of metals that would yield the best properties and also be economical in conjunction with being effective.

2.2 Selection of Metals

2.2.1 Economical Analysis

The main priority while choosing a suitable combination of metals for the concerned anode material was utilizing a combination that is the most economical and has not been tested before for this application. As a result, it was shortlisted down to the following metals: Iron, Copper, Zinc, Aluminium.

Table 1. Economic analysis of various metals

Metals	Conductivity at 25°C (S/m)	Cost ($/kg)
Silver	6.30×10^7	697.0
Copper	5.96×10^7	9.08
Aluminum	3.5×10^7	2.50
Zinc	1.69×10^7	3.64
Nickel	1.43×10^7	25.40
Lithium	1.08×10^7	75.0
Iron	1.00×10^7	0.1357
Cobalt	1.7×10^7	72.40
Tin	9.17×10^6	32.43
Titanium	2.38×10^6	17.0
Tungsten	1.79×10^7	7.28
Molybdenum	1.9×10^7	45.01

Lithium-ion batteries are expensive and so are many other alternatives due to their synthesis methodologies as well as the precursors used. Since an economical product is one of the major objectives, it is important to minimize the cost at the precursor stage. To undertake this, we carried out economic analysis by comparing the prices per weight for each individual major industrial metal. Table 1 shows cost analysis for the major metals employed in industries [17]

2.2.2 Functional Properties Analysis

Functional properties refer to the electrical properties, magnetic, optical properties etc. Of a material that include its performance and ability in different functional devices and applications. In this context, we are concerned with the electrical properties majorly and the metal's overall performance in an energy storing device such as its stability in the electrolytic media and corrosive tendencies as well its reversibility, capacity etc. Regarding this, lead is already being utilized in lead acid batteries. Moreover, there are concerns over its high toxicity as it poses a danger to human health and the environment. Aluminium is already being worked upon by a team of researchers in our institute. To the best of our knowledge, there has been no studies on the combination of Iron and Copper. These are undoubtedly the two most popular and industrially prevalent

metals due to their abundance as well as their exceptional mechanical and functional properties.

2.2.3 Variable Factors and Parameters

We have many different factors to consider while optimizing the synthesis of our active material. After selecting the Fe-Cu combination, it is also important to test various parameters that affects its synthesis and microstructure and properties a whole. For this purpose, 5 different ratios, including a Mono Copper Selenide product with zero presence of any Iron, were selected namely 1:1, 1:2, 1:3 and 1:4 (for Cu:Fe). Iron is shown to be relatively more miscible than Copper and therefore, an increasing iron percentage is adopted. An increasing copper percentage would lead to incomplete dissolution of copper in mixture rendering the synthesis difficult. Besides the molar ratios, the Selenization time and temperature can also be adjusted and varied accordingly for an optimized synthesis route. For the scope of our thesis, we are concerned with the differing molar ratios only. This methodology of altering both the concentration of the reactants as well as the surfactant CTAB has been observed [14].

2.2.4 Calculation of Molar Ratios

Each solution of precursors so produced consisted of 2 moles of the metallic salts in total. All ratios were produced within this 2 moles constraint. The moles of each precursor were converted into milligrams and tabulated for ease in weighing the amounts. The calculated values of each individual component are given in Table 2.

2.3 Phase 1: Solution Method

2.3.1 Preparation of solutions

Precursors:

Copper pentahydrate sulphate ($CuSO_4.5H_2O$)

Iron heptahydrate sulphate ($FeSO_4.7H_2O$)

Reducing Agent: Sodium borohydride ($NaBH_4$)

Solvent: Deionized water

Surfactant: Cetyltrimethylammonium bromide (CTAB)

Each key component played its own role and was added in precise amounts. Two solutions were prepared. Solution A consisted of 50mL D.I. water along with 2 moles of the sulphate salts (as per the molar ratios for the specific sample so being produced) and 500 mg of CTAB as surfactant, as per literature data. Solution B consisted of 100 mg NaBH4 dissolved in 10mL D.I. water. All components were stirred with a magnetic stirrer on a hot plate at room temperature.

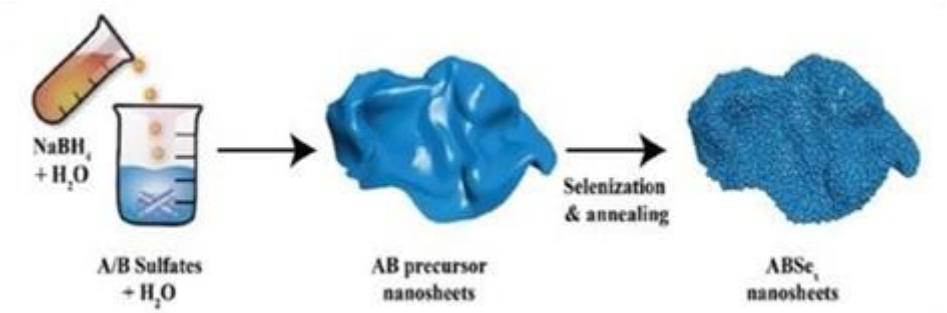

Fig. 2. General schematic of the synthesis process. (Ref: doi: 10.1002/smll.201901995)

2.3.2 Reduction of Sulphates

Solution B was then added dropwise into Solution A whilst Solution A was being stirred vigorously on the hot plate. The speed of revolution was 1300 RPM. On completely adding Solution B into A, the now produced solution was allowed to be stirred for 8-10 minutes further.

2.3.3 Washing & Drying

The reduced solution was then carried through the washing process. The 60 mL solution was divided into 4 15mL falcon tubes. The solution was added in partial amounts sequentially into each tube so as to ensure a balance in the amounts of precipitates transferred. 4 centrifuge cycles of 10 mins each were carried out at 4500 RPM and 25^{o}C. The first cycle segregated the particles while the subsequent cycles involved washing with ethanol and water in alternating cycles.

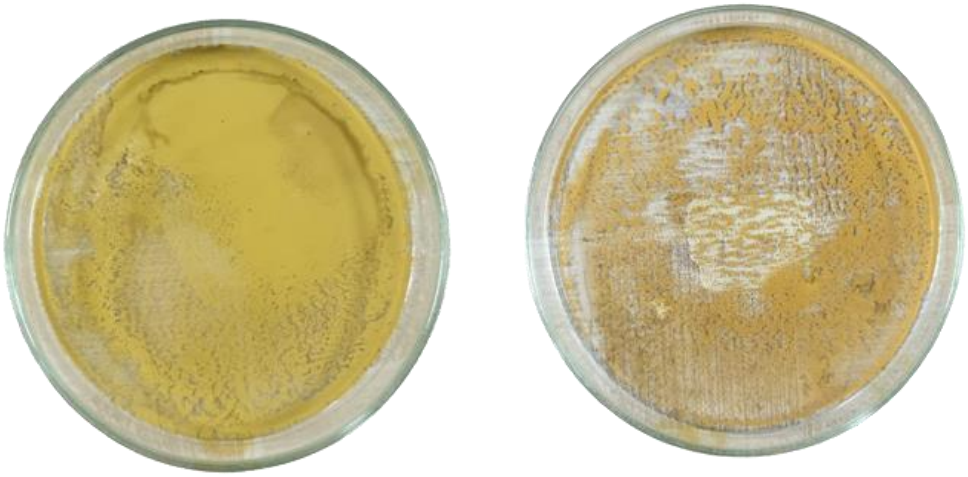

(a) (b)

Fig. 3. Reduced, washed and dried Cu-Fe sample in the ratio (a) 1:1 (b)1:2

The washed powder samples were in falcon tubes were drained of the ethanol and dried in a vacuum oven for 12 hours at 60^{o}C. The resulting dried samples were then taken for the second phase of synthesis i.e. Selenization.

2.4 Phase 2: Selenization

2.4.1 Preparation of sample

Selenization is the reaction of the reduced powder sample with the Selenium powder. The Selenium powder and the reduced Sulphates powder were weighed in a weighing balance with more than 100 mg of the reduced powder and Selenium powder with double the amount i.e. with a 1:2 ratio (Reduced Sulphate: Selenium). These were then placed at opposite ends of an Alumina boat with the powder spread out for increased reaction kinetics. The reaction was carried out in a tube furnace in a H_2/Ar atmosphere (with 10% H_2 by volume). The reducing gas flow was kept at a steady stable rate so as to not cause turbulent flow and also keep the reaction running. The gas was introduced from the Selenium side of boat.

2.4.2 Heating

The heating cycle was carried out over a period of 9.5 hours. First, the temperature was increased at a ramp rate of 4C/min till it reached 300C. This is where the

major reaction occurred. This involved an exchange reaction of Selenium with the Oxides and Alkoxides in the particles. It was held at this temp for 4 hours. After this, it was again increased at a rate of 5C/min and held at 400C for 1.5 hours for annealing. The annealing allows for the fine and uniform dispersion of Selenium throughout the mix of Alkoxides and Oxides. It was then allowed to cool to room temperature.

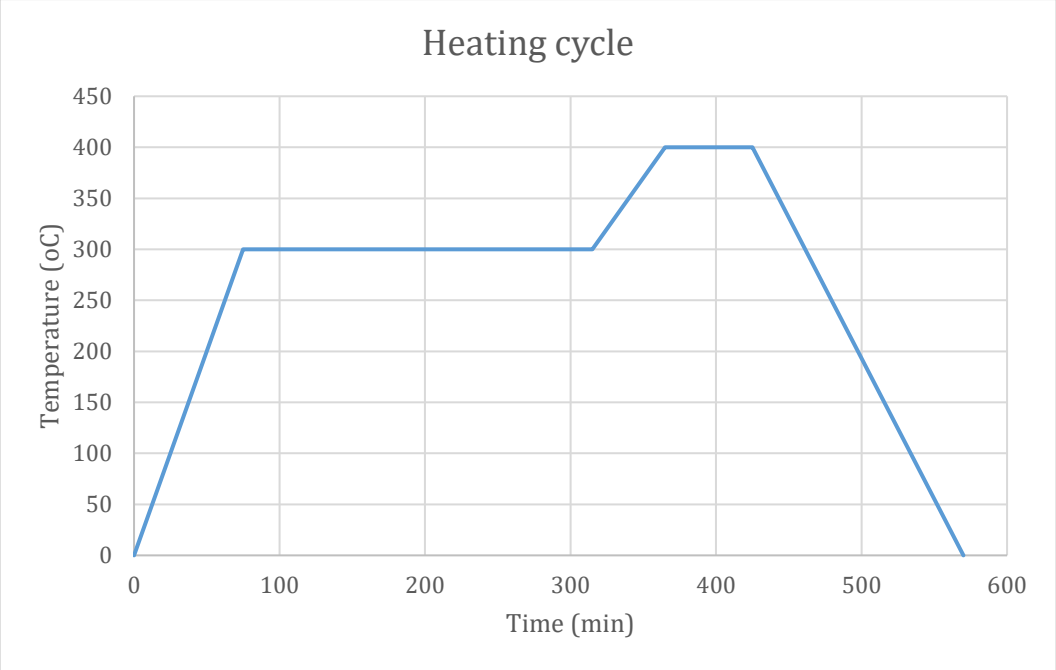

Fig. 4. Heat treatment cycle for Selenization

2.4.3 Separation of Selenides

Following the reaction, the boat was taken out and the final Selenide product was observed at one side of the boat along with unreacted Se with impurities on the other side. The separation of these two components was not required and hence, it was easy to get the black Selenide powder.

Fig. 5. Copper Selenide powder sample (left) with unreacted silvery mass of Selenium with impurities (right)

2.5 Characterization

2.5.1 X-Ray Diffraction Spectroscopy

XRD Analysis for all selenide ratios was carried out in a standard XRD equipment with a Cu anode target as the Kα ray source at Keele University, Keele, UK. MDI Jade was used for peak matching and indexing. The purpose of the XRD Analysis was to identify all major phases of Iron and Copper present as well as observing whether the ratios of Iron and Copper were maintained post-reaction.

2.5.2 Scanning Electron Microscopy

Scanning Electron Microscopy was carried out for both the pre-Selenized as well as Selenized product. The analysis of pre-Selenized samples was carried out at School of Chemical and Materials Engineering, NUST, Islamabad while the Selenized samples were analysed at Keele University, Keele, UK. The purpose of SEM analysis was to observe morphology of the obtained 2D nanostructure and determine the ideal ratio of precursors that corresponds to the ideal formation.

2.5.3 BET Analysis

BET analysis was carried out at SCME, NUST, Islamabad to determine the BET-specific surface areas of the obtained nanostructures through N2 sorption test. They were analysed in gas adsorption analyser at 77K. The samples were evacuated for 3 hours at 150^{o}C before the adsorption tests [11]. All graphs were plotted on Origin.

2.6 Electrochemical Testing

2.6.1 Preparation of Electrode

The selenide powder was formed into an anode by weighing 75mg of the selenide along with 15mg CMC as binder and 15mg Carbon black for increased conductivity. These three powders were mixed and ground using a mortar and press. Around 10mL of D.I. water was added to form slurry.

2.6.2 Three Electrode Testing

The slurry was casted on glassy Carbon substrate. This acted as the working electrode in our 3-electrode system. The reference electrode was a Ag/AgCl system while Platinum was used as the counter electrode. oil and then cut into 10mm discs. The anode discs were then assembled with a separator, cathode, electrolyte, and spacer on a coin pressing machine.

2.6.3 Cyclic Voltammetry and GCD Analysis

The 3-electrode system was connected with an electrochemical testing station and cyclic voltammetry was carried out over 6 cycles. The purpose was to determine whether the system exhibited capacitive or EDCL behaviour and also to determine the potentials of the reactions occurring. It was carried out at SINES, NUST.

Galvanostatic Charge Discharge Analysis was carried out to determine the charging-discharging behaviour of the active material and calculate its electrode capacity.

CHAPTER 3

RESULTS AND DISCUSSION

3.1 Characterization

For the characterization of the materials, SEM and XRD are the basic requirements to confirm the identity as well as to obtain the structural information of the sample. XRD results provided us with the information regarding the crystal structures existing in our samples along with the phase identification. SEM provided the morphological analysis to confirm the 2D nano-sheet like structure of the particles. Afterwards, BET was also conducted to find out the specific surface area of the samples. A very high surface area leads to higher electrochemical interface between the active anode material and the electrolyte solution. This results in a greater charge storage capacity and conductivity.

3.1.1 SEM

We can investigate the SEM images of 5 different molar ratios of our samples. The objective was to achieve a sheet like structure prior to selenization for which different molar ratios of the metallic precursors were used. Once the sheet like structure was obtained, it was possible to maintain that structure after Selenization as well.

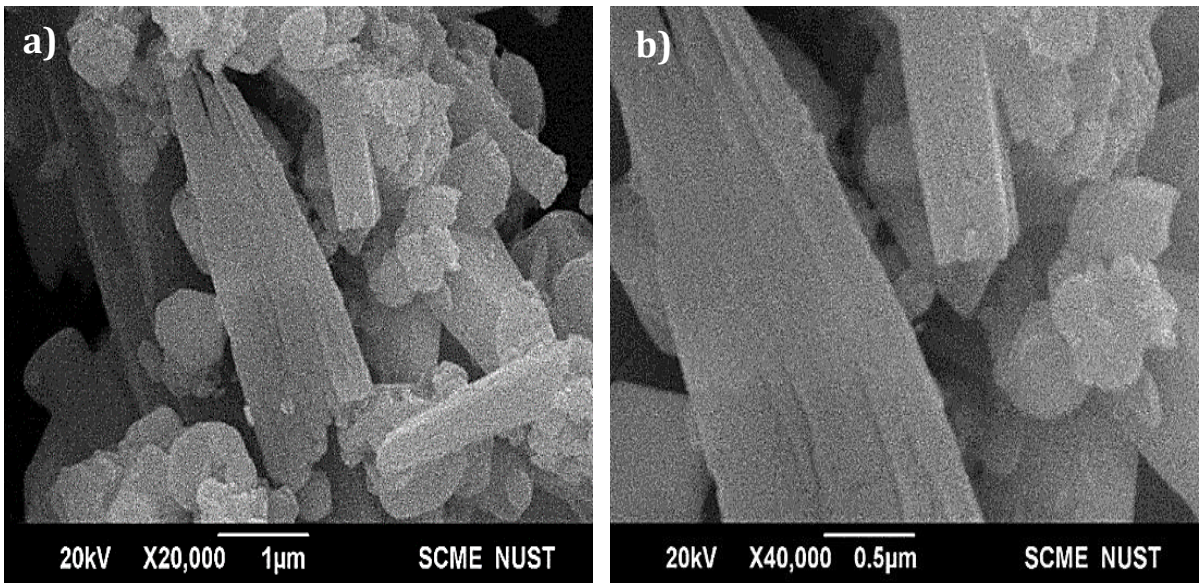

Fig. 6. SEM images for Mono Copper precursors at (a)20,000X (b)40,000X

The SEM images in Fig. 6 show the particle morphology for Mono Copper precursor sample. The images at different magnifications clearly show a thick coarse plate like structure which is not needed and can be hypothesized to give a smaller surface area than the sheet like morphology which was later confirmed with the BET analysis as well. It can also be observed that the size distribution of the plates is not uniform either, which is also not something that we wanted out of our sample because that might result in weakness in structural integrity when the sample would be subjected to charge-discharge cycles and undergo volumetric changes.

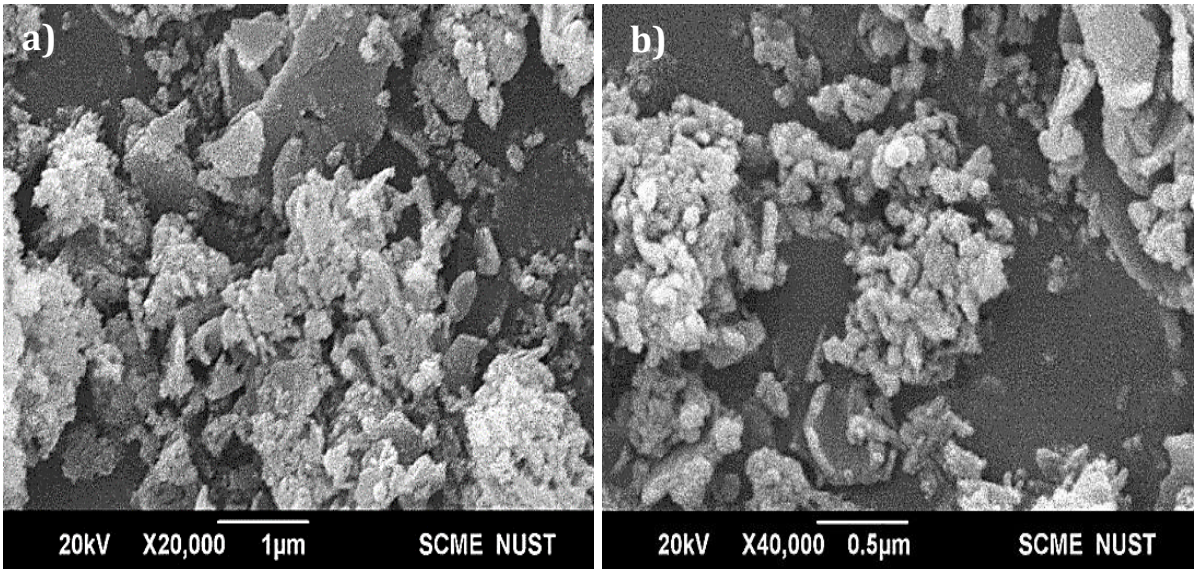

Fig. 7. SEM images for 1:1 Copper-Iron precursors at (a)20,000X (b)40,000X

The SEM images in fig. 7 show an irregular particulate morphology. At x20000, we can see a lot of bigger particles as well as smaller particles in random orientations. There is no particular shape that can be designated to this structure and again the particles are varying in size. Structural homogeneity was required to effectively study the effect of the particle shape on the electrochemical performance of the material. Hence, such variations were not suitable to get any reliable results.

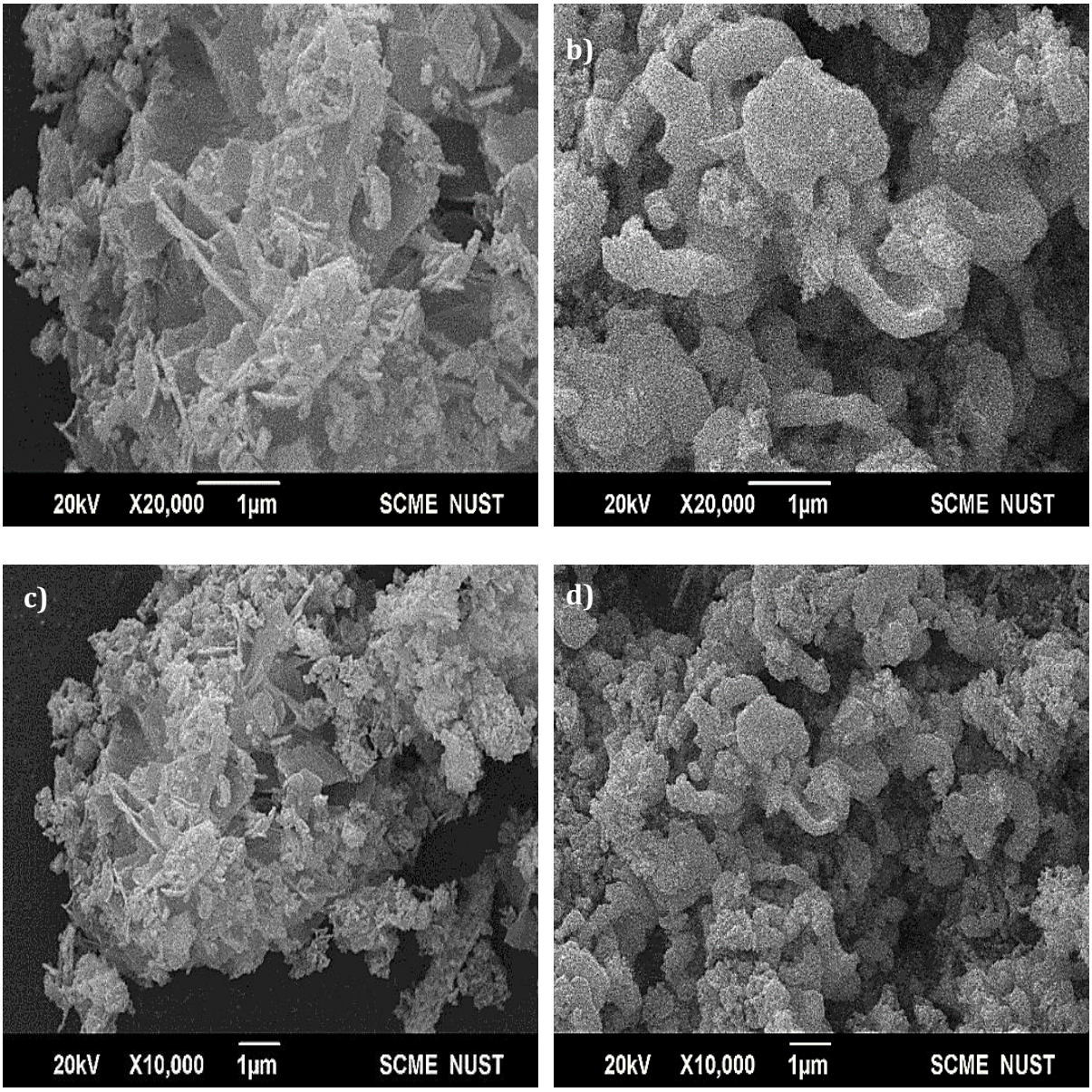

Fig 8. SEM Images of 1:2 Copper-Iron (a) Precursor at 20,000X (b) Selenide at 20,000X (c) Precursor at 10,000X (d) Selenide at 10,000X

The SEM images in figure 8a and 8c show the sample morphology for 1:2 composition of metallic precursors and the images 3b and 3d are the Selenized products of these samples. Pre-Selenized samples exhibit a fine sheet like structure which can be observed by seeing thin structures oriented in different directions. The Selenized product in contrast shows a coarser and rounder structure. Hence, with the initial objective being accomplished of achieving a 2D structure of the precursor, the Selenization cycle can be optimized to preserve that post reaction as well. Another good thing to notice here is the fact that the sheet like structure is homogeneous throughout the image.

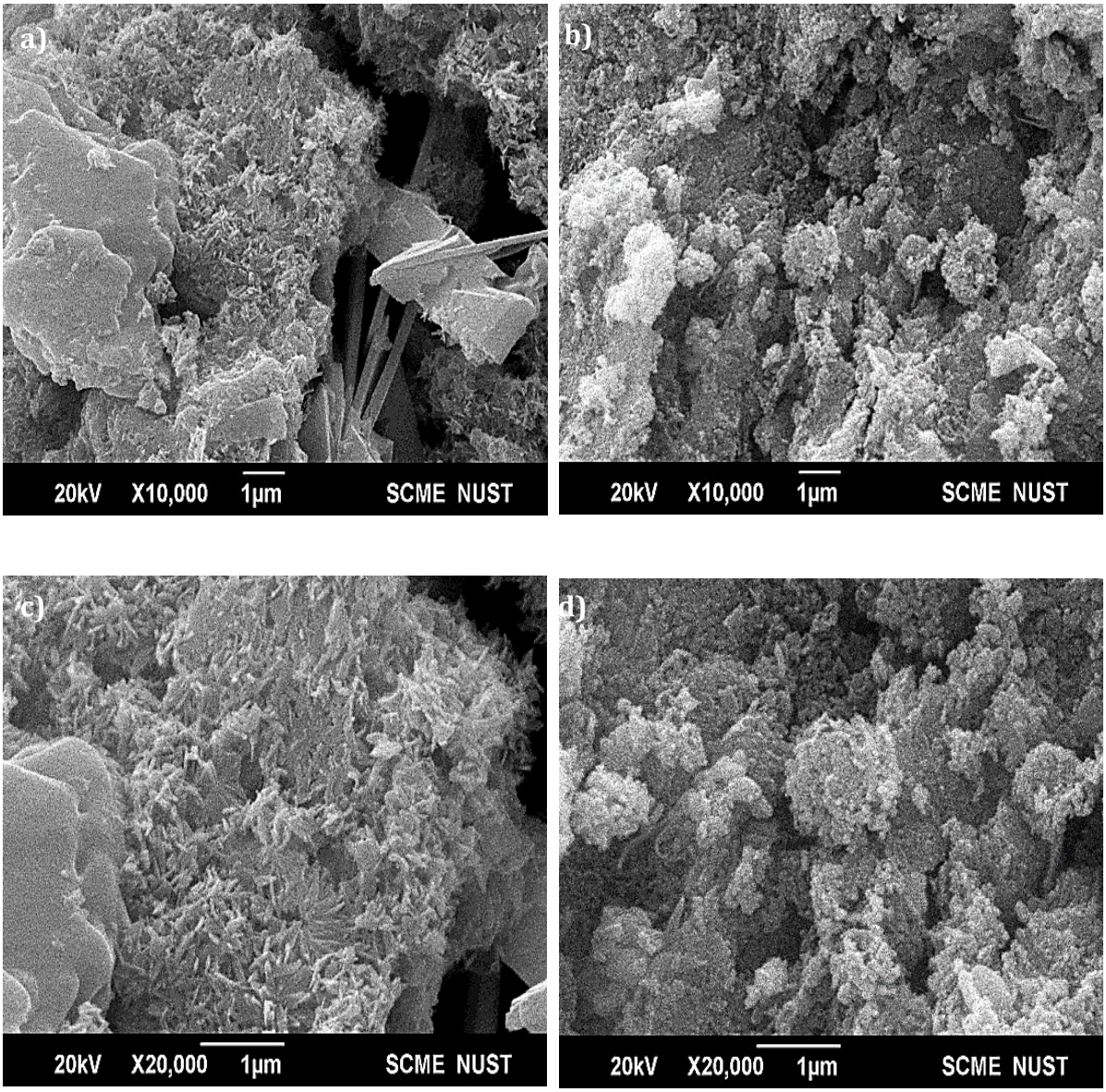

Fig 9. SEM Images of 1:3 Copper-Iron (a) Precursor at 10,000X (b) Selenide at 10,000X (c) Precursor at 20,000X (d) Selenide at 20,000X

Here, the SEM images before and after selenization for the 1:3 sample can be observed at two different magnifications. Such structures are not required as we can clearly see in the lower magnification images, the sample prior to reaction exhibits a variety of different particle structures where we can see a needle like structure in one region, along with some rod like structures as well as agglomerated particles. This morphology was not suitable for our objectives. And the post selenization images also show rough irregular particles being formed. Hence, this particular sample ratio was not suitable on the basis of particle structure.

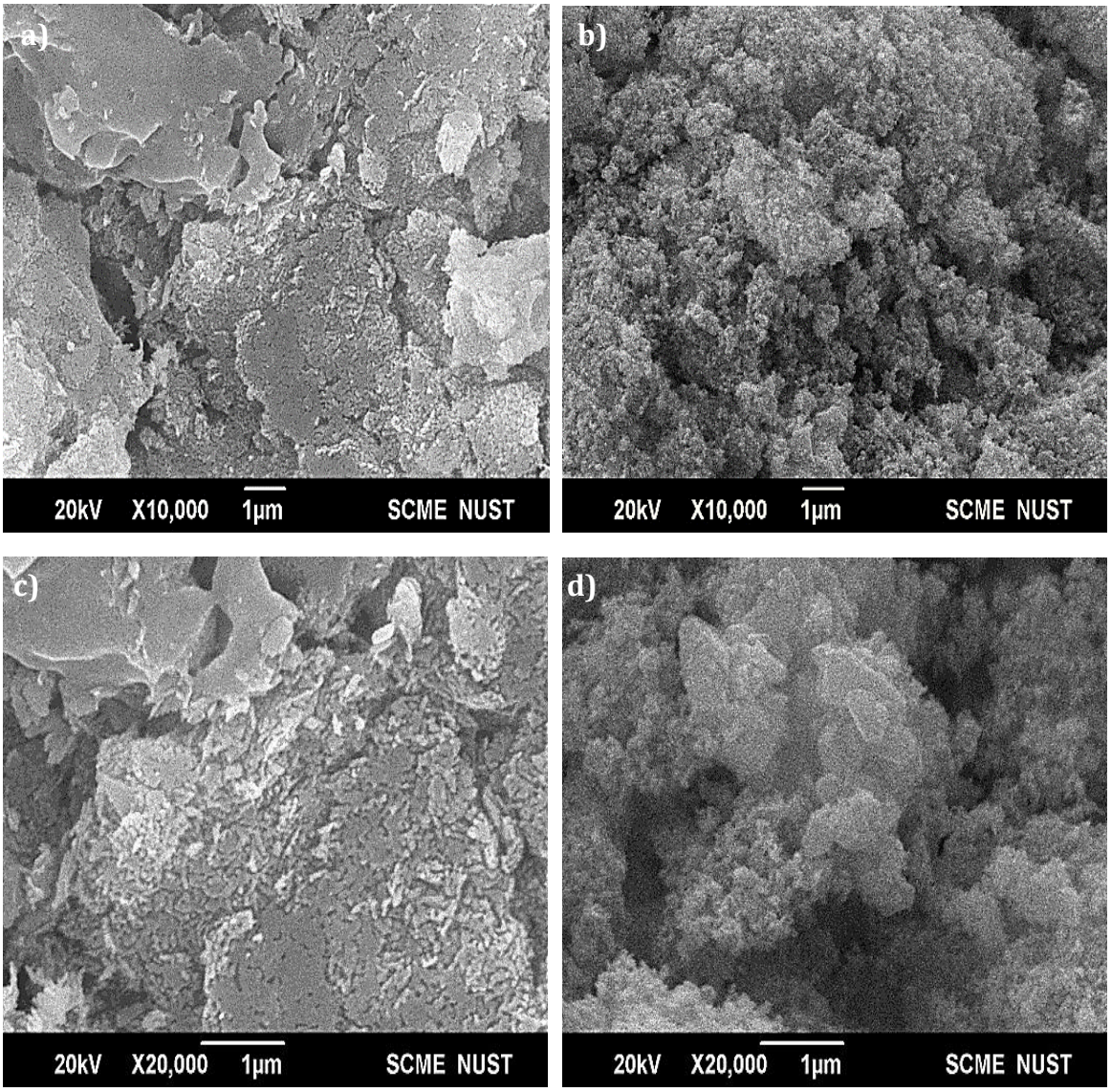

Fig 10. SEM Images of 1:4 Copper-Iron (a) Precursor at 10,000X (b) Selenide at 10,000X (c) Precursor at 20,000X (d) Selenide at 20,000X

For this particular ratio, again we can see agglomerated particles of relatively larger sizes for the precursors of the sample. And for the Selenized product, the morphology is random particle like.

From the morphological analysis, we concluded that the 1:2 sample gives the optimum shape but the Selenized product still gives an unfavourable morphology which can be optimized by adjusting the reaction cycle.

3.1.2 X-ray diffraction spectroscopy

X-ray diffraction spectroscopy was conducted to investigate the crystal structure and lattice parameters of the phases present in our sample. During the time frame of this project, the XRD analysis of 3 samples was possible, namely the Mono Copper Selenide, 1:2 and 1:3 Copper Iron Selenide.

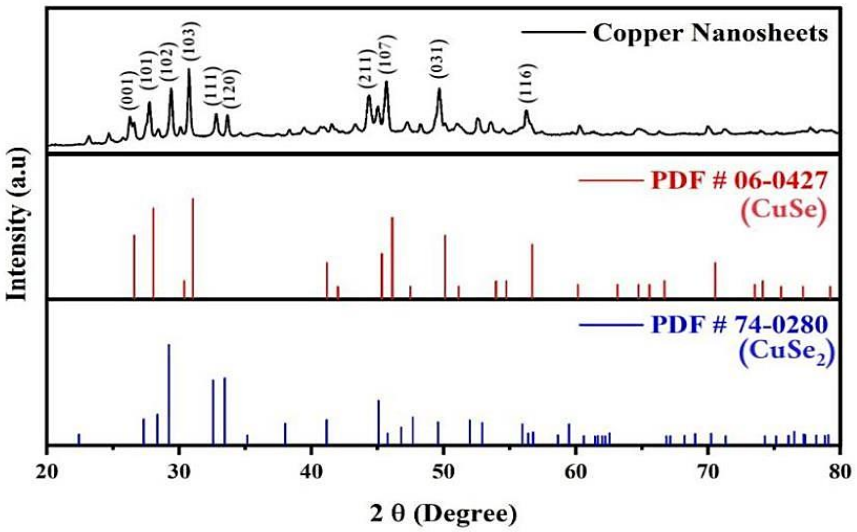

Fig. 11. XRD for Copper Selenide

The XRD pattern showed major peak matching with the 'Klockmanite' phase of CuSe that exhibits a hexagonal structure. The major peaks that match with the PDF# 06-0427 are the (001), (101), (103), (107), (031) and (116). A few minor peaks matched with a separate phase of $CuSe_2$ from the PDF# 74-0280 which are indexed as (102), (111) and (211), existing in the orthorhombic phase.

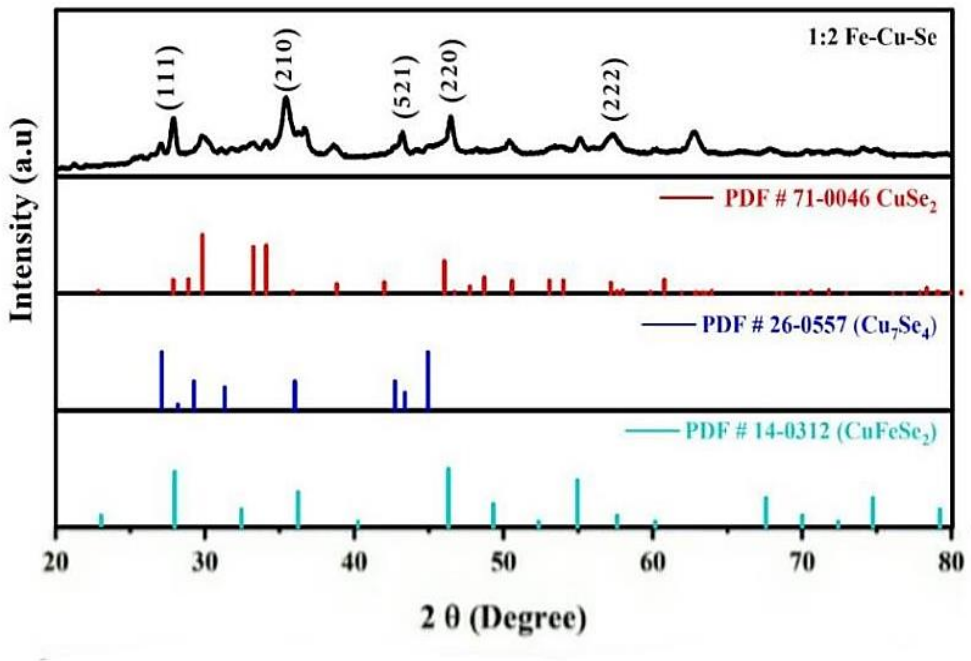

Fig. 12. XRD for 1:2 Copper-Iron Selenide

Major peak matching with the 'Eskeborite' phase of $CuFeSe_2$ can be seen along the planes (111), (210) and (220) in fig. 7 for the 1:2 sample. This is a simple cubic structure with a lattice parameter of 5.53 Å. Some auxiliary peaks were designated to separate phases of Copper selenide as well. The good thing exhibited in these XRD patterns are the fact that there are no impurity peaks which suggests the reaction occurred completely without any contamination during handling of the sample.

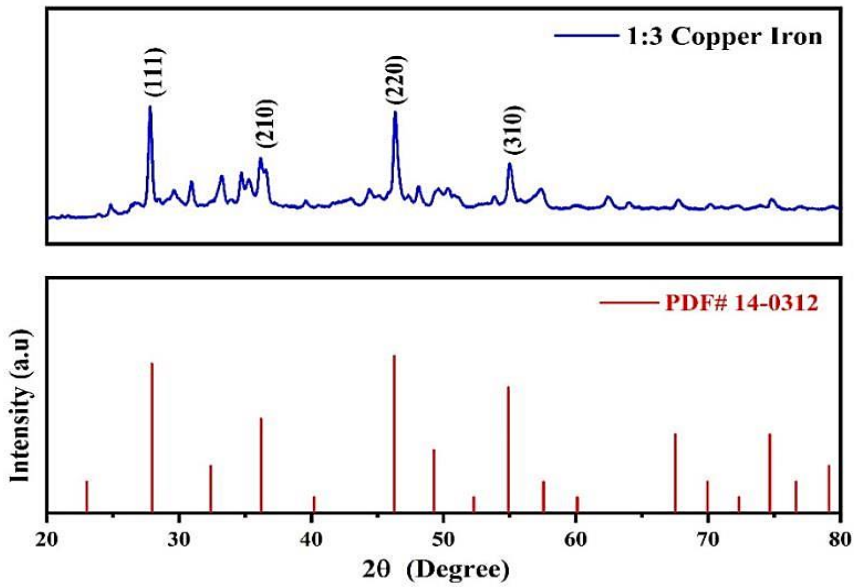

Fig. 13. XRD for 1:3 Copper-Iron Selenide

For the sample 1:3 Copper-Iron Selenide, the major peak matching is achieved with the 'Eskeborite' phase $CuFeSe_2$ which is consistent with the 1:2 sample, which is a good sign that the reaction is proceeding in a similar manner for different ratios and hence a similar phase is achieved. Major peak matching is achieved along the planes (111), (210) and (310). Again, a cubic structure is achieved with a lattice parameter of 5.53 Å.

During the XRD, the crystallite size of the samples can be calculated from the Scherrer equation which is as follows:

$$D = 0.9\lambda/\beta Cos\theta$$

; Where

λ – The wavelength of the incident x-ray θ- the diffraction angle at FWHM β- Full width at half maximum (FWHM)

3.1.3 BET

BET was conducted to calculate the specific surface area of the samples. It is worth noting that the BET graphs that follow only show an adsorption peak while the

typical BET plots are full isotherms consisting of both the adsorption as well as the desorption peak. For our sample, we do not require the information from desorption peak as we are not concerned with the pore volume and pore width of the samples. Hence a 5-point BET adsorption curve for the surface area will suffice. Through the duration of our project, we were able to conduct BET of two sample ratios, 1:1 and 1:2 Copper-Iron Selenide.

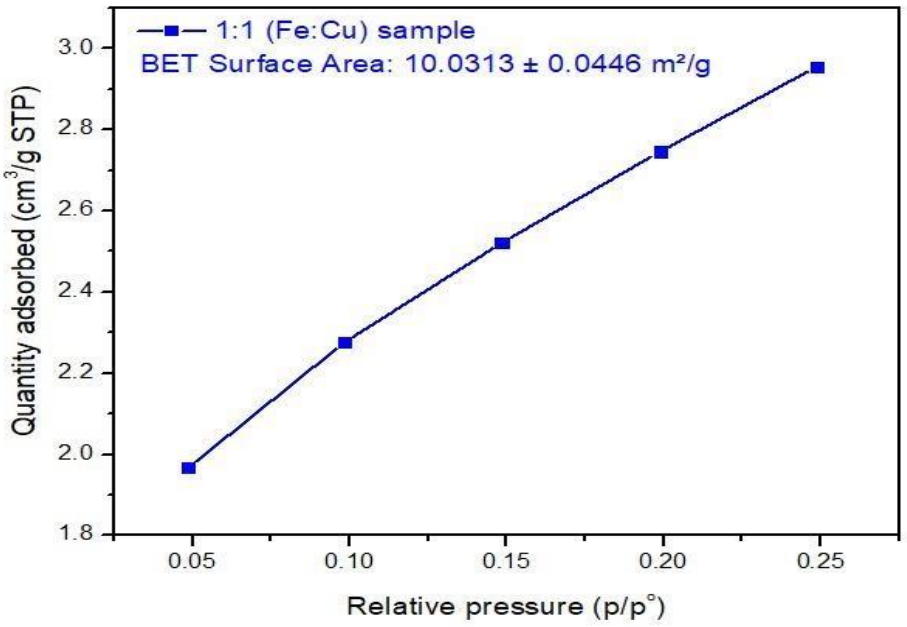

Fig. 14. The BET adsorption curve for 1:1 Cu:Fe sample

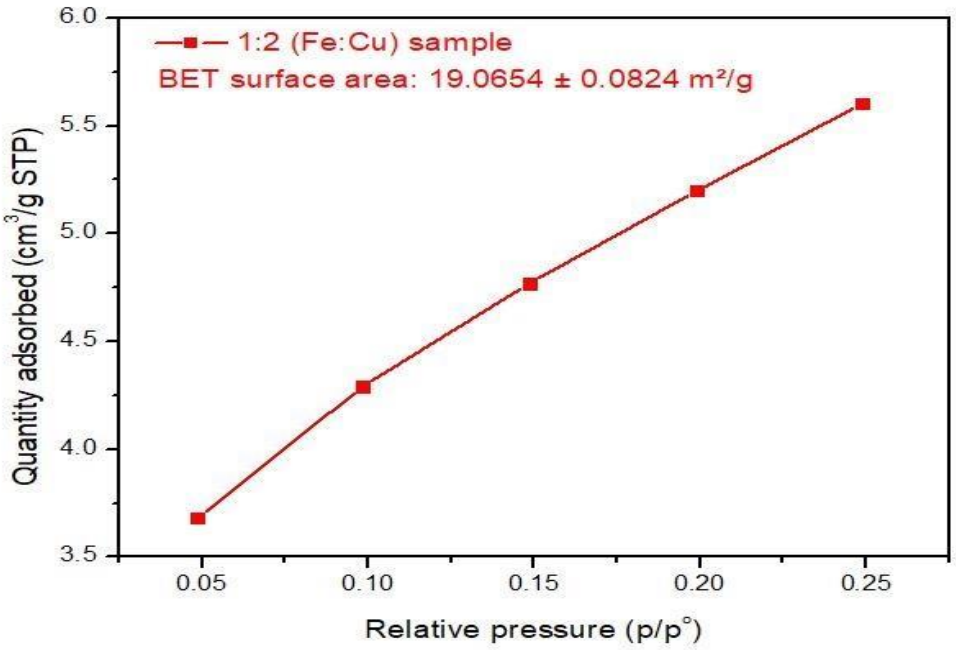

Fig. 15. The BET adsorption curve for 1:2 Cu:Fe sample

The BET analysis of the 1:1 sample exhibited a 10.0313 m^2/g of BET surface area while the 1:2 sample exhibited almost double the surface area at 19.0654 m^2/g. The electrochemical performance of the material has a direct relation with the surface area of the sample. A greater surface area will provide a greater electrochemical interface between the electrode and the electrolyte, hence a greater number of reaction sites will be available for the conversion mechanism to occur.

3.2 Electrochemical testing

The final phase of the project was to conduct electrochemical testing of the material. The 1:2 ($CuFeSe_2$) sample provided optimum morphology hence that sample was chosen for testing. Cyclic voltammetry and Galvanostatic charge discharge testing was carried out for the material in a 3 electrode system, with a Silver Chloride reference electrode and Platinum counter electrode. Originally, the electrode material was to be tested with Sodium ion electrolyte but due to the unavailability of glove box, Zinc Sulphate had to be used to test the performance of the material.

3.2.1 Cyclic voltammetry

The CV test was carried out in the potential window -0.4V to 0.7V on an electrochemical testing station. The plots were plotted on Origin. Six different potentials denoted by the different colours are shown against the

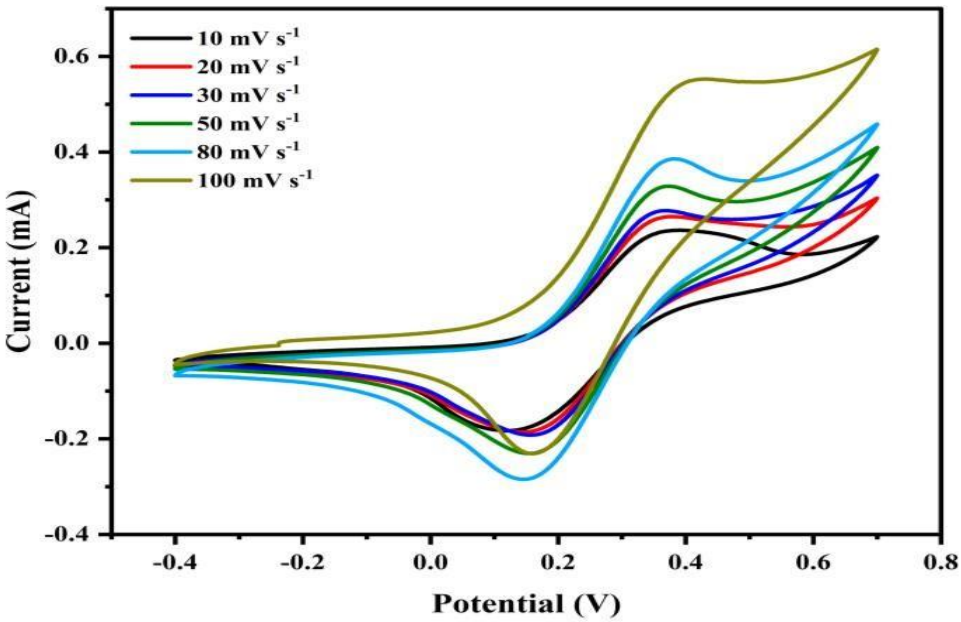

Fig. 16. The CV curves for 1:2 sample

The resulting current from different scan rates is depicted in the CV curve. The curve shows oxidation and reduction peaks corresponding to the charging and discharging mechanism. The curve deviates from a rectangular behaviour, hence it provides a pseudo capacitive response to the voltage stimulus. It can also be noticed that for increasing scan rate, the resulting current is also increasing.

3.2.2 Galvanostatic charge discharge

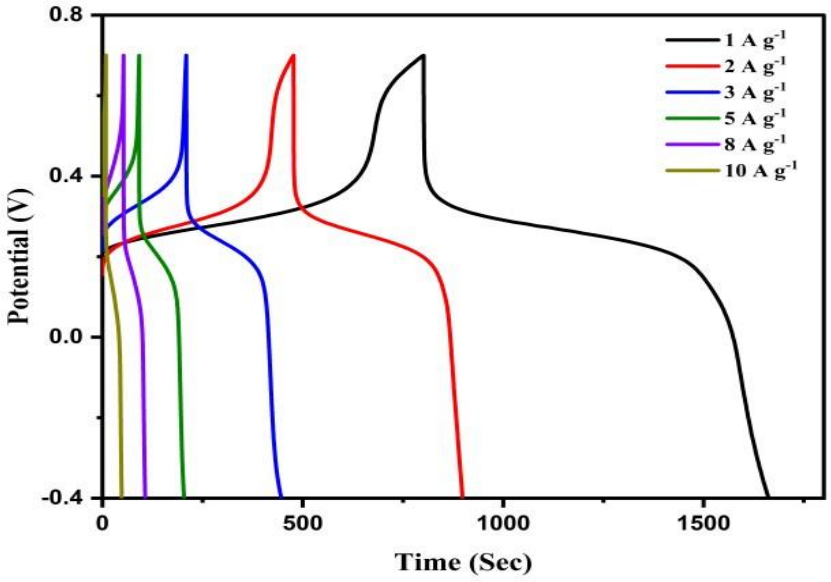

Fig. 17. GCD curves for 1:2 sample

Galvanostatic charge discharge was used at different current rates to find out the specific capacities of the material. For different current rates, the sample exhibits a plateau at the same voltage where the CV plot exhibits the redox reaction. GCD makes a graph of voltage against time for the charge discharge behaviour, which is then used in the relationship given below to find out the specific capacity:

$$C = \frac{I * t}{m * V}$$

; Where

C – Capacity I – Current density m – Mass of the sample

V – Voltage drop during discharge t – Discharge time

Table 2. Specific capacitances for various current densities and their respective discharge times.

Current density (Ag^{-1})	**Discharge time (s)**	**Potential (V)**	**Specific capacitance (Ahg^{-1})**
1	863.09	1.1	784.627
2	421.95	1.1	767.18
3	305.64	1.1	933.563
5	181.42	1.1	824.636
8	101.99	1.1	741.745
10	76.67	1.1	697

The specific capacitance value peaks out for a current density of 3 Ag^{-1}.

CONCLUSION

To conclude, we can argue that the 1:2 $CuFeSe_2$ sample gave a favourable morphology and reasonable XRD results. When subjected to the electrochemical testing of this sample, the material exhibited pseudo capacitive (might even be hybrid battery) nature. Further testing is still required such as rate capability, cyclic stability and electrochemical impedance testing. Furthermore, if the Selenization cycle can be optimized to preserve the initial 2D structure of the material, even better results can be achieved. Also, the material needs to be tested with Sodium ion electrolyte to fulfil the purpose of the project in the future. A reliable setup for new age batteries will take the energy sector into a new age of sustainable growth.

BIBLIOGRAPHY

[1] A. Capon, "Can Lithium Supply Keep Up With Strong EV Demand?," (2021). https://www.institutionalinvestor.com/article/b1sdwwdh7zqkxl/canlithium-supply-keep-up-with-strong-ev-demand (accessed May 28, 2022).

[2] K. Chayambuka, G. Mulder, D. L. Danilov, and P. H. L. Notten, "Sodium-Ion Battery Materials and Electrochemical Properties Reviewed," *Adv. Energy Mater.*, vol. 8, no. 16, pp. 1–49, (2018), doi: 10.1002/aenm.201800079.

[3] A. Jana, R. Paul, and A. K. Roy, *Architectural design and promises of carbon materials for energy conversion and storage: In laboratory and industry*. Elsevier Inc., (2019).

[4] N. Yabuuchi, K. Kubota, M. Dahbi, and S. Komaba, "N. Yabuuchi, K. Kubota, M. Dahbi, S. Komaba, Research Development on Sodium-Ion Batteries, Chem. Rev. 114 (2014) 11636-11682," *Chem. Rev.*, vol. 114, no. 23, pp. 11636–11682, (2014), [Online]. Available: http://www.ncbi.nlm.nih.gov/pubmed/25390643.

[5] Z. Liu, T. Lu, T. Song, X. Y. Yu, X. W. Lou, and U. Paik, "Structure-designed synthesis of FeS2@C yolk-shell nanoboxes as a high-performance anode for sodium-ion batteries," *Energy Environ. Sci.*, vol. 10, no. 7, pp. 1576– 1580, (2017), doi: 10.1039/c7ee01100h.

[6] W. Choi, N. Choudhary, G. H. Han, J. Park, D. Akinwande, and Y. H. Lee, "Recent development of two-dimensional transition metal dichalcogenides and their applications," *Mater. Today*, vol. 20, no. 3, pp. 116–130, (2017), doi: 10.1016/j.mattod.2016.10.002.

[7] Z. Hu, Q. Liu, S. L. Chou, and S. X. Dou, "Advances and Challenges in Metal Sulfides/Selenides for Next-Generation Rechargeable Sodium-Ion Batteries," *Adv. Mater.*, vol. 29, no. 48, pp. 1–24, (2017), doi: 10.1002/adma.201700606.

[8] Z. Tang, Z. Zhang, Y. Wang, S. C. Glotzer, and N. A. Kotov, "Self-assembly of CdTe nanocrystals into free-floating sheets," *Science (80-.).*, vol. 314, no. 5797, pp. 274–278, (2006), doi: 10.1126/science.1128045.

[9] C. Schliehe *et al.*, "Ultrathin PbS sheets by two-dimensional oriented attachment," *Science (80-.).*, vol. 329, no. 5991, pp. 550–553, (2010), doi: 10.1126/science.1188035.

[10] H. Duan *et al.*, "Ultrathin rhodium nanosheets," *Nat. Commun.*, vol. 5, pp. 1– 8, (2014), doi: 10.1038/ncomms4093.

[11] S. Zeng *et al.*, "Synthesis of symmetrical hexagonal-shape PbO nanosheets using gold nanoparticles," *Mater. Lett.*, vol. 67, no. 1, pp. 74–77, (2012), doi: 10.1016/j.matlet.2011.09.048.

[12] Z. Li *et al.*, "Synthesis of single-crystal gold nanosheets of large size in ionic liquids," *J. Phys. Chem. B*, vol. 109, no. 30, pp. 14445–14448, (2005), doi: 10.1021/jp0520998.

[13] W. Cheng, S. Dong, and E. Wang, "Synthesis and Self-Assembly of Cetyltrimethylammonium Bromide-Capped Gold Nanoparticles," *Langmuir*, vol. 19, no. 22, pp. 9434–9439, (2003), doi: 10.1021/la034818k.

[14] Z. Khan, T. Singh, J. I. Hussain, and A. A. Hashmi, "Au(III)-CTAB reduction by ascorbic acid: Preparation and characterization of gold nanoparticles," *Colloids Surfaces B Biointerfaces*, vol. 104, pp. 11–17, (2013), doi: 10.1016/j.colsurfb.2012.11.017.

[15] Z. Ali, T. Zhang, M. Asif, L. Zhao, Y. Yu, and Y. Hou, “Transition metal chalcogenide anodes for sodium storage,” *Mater. Today*, vol. 35, no. xx, pp. 131–167, (2020), doi: 10.1016/j.mattod.2019.11.008.
[16] Z. Ali, M. Asif, T. Zhang, X. Huang, and Y. Hou, “General Approach to Produce Nanostructured Binary Transition Metal Selenides as HighPerformance Sodium Ion Battery Anodes,” *Small*, vol. 15, no. 33, pp. 1–10, (2019), doi: 10.1002/smll.201901995.
[17] “Commodity Prices | Commodity Market | Market Insider” (2022). https://markets.businessinsider.com/commodities (accessed May 15, 2022).